

**Manuscript version: Author's Accepted Manuscript**

The version presented in WRAP is the author's accepted manuscript and may differ from the published version or Version of Record.

**Persistent WRAP URL:**

<http://wrap.warwick.ac.uk/148752>

**How to cite:**

Please refer to published version for the most recent bibliographic citation information. If a published version is known of, the repository item page linked to above, will contain details on accessing it.

**Copyright and reuse:**

The Warwick Research Archive Portal (WRAP) makes this work by researchers of the University of Warwick available open access under the following conditions.

Copyright © and all moral rights to the version of the paper presented here belong to the individual author(s) and/or other copyright owners. To the extent reasonable and practicable the material made available in WRAP has been checked for eligibility before being made available.

Copies of full items can be used for personal research or study, educational, or not-for-profit purposes without prior permission or charge. Provided that the authors, title and full bibliographic details are credited, a hyperlink and/or URL is given for the original metadata page and the content is not changed in any way.

**Publisher's statement:**

Please refer to the repository item page, publisher's statement section, for further information.

For more information, please contact the WRAP Team at: [wrap@warwick.ac.uk](mailto:wrap@warwick.ac.uk).

# Modelling and interaction analysis of the self-pierce riveting process using regression analysis and FEA

Huan Zhao<sup>a</sup>, Li Han<sup>b</sup>, Yunpeng Liu<sup>a</sup> and Xianping Liu<sup>a,\*</sup>

<sup>a</sup> School of Engineering, University of Warwick, Coventry CV4 7AL, UK

<sup>b</sup> Hansher Consulting Ltd., Coventry, UK

\* X.Liu@warwick.ac.uk

## Abstract:

Self-pierce riveting (SPR) is a major joining method used in the automotive industry. However, there still lacks a fast and easy-to-use joint quality prediction tool available for the automotive engineers. In this study, the simple but effective regression analysis method was applied to quickly predict the SPR joint quality. Two regression models were developed for the prediction of the interlock and the minimum remaining bottom sheet thickness ( $T_{\min}$ ). The prediction accuracy of the developed regression models was validated by comparing with the experimental results. Under the studied joint configurations, the mean absolute errors (MAE) of the interlock and  $T_{\min}$  were 0.047mm and 0.053mm respectively, and the corresponding mean absolute percentage errors (MAPE) were 10.4% and 12.3%. With the developed models, the interaction effects between rivet and die parameters on the joint interlock and  $T_{\min}$  were also systematically analysed. The results revealed that the rivet and die parameters demonstrated significant influences on the interlock but not on the  $T_{\min}$ . These interaction effects were further examined by analysing the deformations of the rivet and substrate materials. Moreover, the die-to-rivet volume ratio ( $R$ ) was found to be critical for the formation of interlock, and a larger interlock is more likely achieved when the  $R$  is close to 1.0.

**Keywords:** SPR; Multiple regression model; Interaction effect; Rivet length; Die geometry; Die-to-Rivet volume ratio

# 1 Introduction

With the increasing applications of light-weight materials, especially aluminium alloys, in body-in-white (BIW) structures, self-pierce riveting (SPR) has become one of the major connection methods in the automotive industry [1]. As a mechanical joining approach, SPR is capable of connecting two or more layers of similar or dissimilar materials, such as aluminium alloys, magnesium alloys, steels and even composite materials. It can also be applied on parts with coated or painted surfaces and does not require pre-drilled holes [2][3][4][5]. Moreover, the SPR joining system is very convenient to be integrated into the automation production line. Therefore, the SPR technique has been heavily utilized in the automotive aluminium BIW assembly [6, 7].

Taking a two-layer joint as an example, the four steps during SPR process are schematically shown in **Fig. 1**. First, the blank-holder moves downward and clamps the two sheets together. Then, the punch moves downward and presses the rivet into the sheets. The rivet shank first pierces through the top sheet and then flares into the bottom sheet. Finally, the punch and blank-holder are lifted, and a SPR joint with a mechanical interlock is formed. As shown in **Fig. 2**, the SPR joint quality is usually assessed by three critical indicators measured on the joint cross-sectional profile: (1) the interlock; (2) the minimum remaining bottom sheet thickness ( $T_{\min}$ ) and (3) the rivet head height [8]. The interlock is critical for the mechanical strengths and failure behaviours of SPR joints. Too small interlock values may result in pull-out failure of the rivet shank from the bottom sheet [9]. The  $T_{\min}$  is very important for the corrosion resistance and water-proof performance of SPR joints. If the  $T_{\min}$  was 0.0 or negative, moisture or water invasion would inevitably occur in service. This will accelerate corrosion between the steel rivet and the aluminium sheets, and result in premature corrosion failure of SPR joints. Zhang et al. [10] also reported that fatigue failure may occurred on the bottom sheet if the  $T_{\min}$  was very small. The rivet head height not only influences cosmetic appearance of the connected structure but also the joint corrosion resistance. A protruded rivet head usually causes gaps between the rivet and the connected sheets, and thus increases the moisture or water invasion problem. The rivet head height also directly links with the final position of the rivet inserted into the sheets and thus affects the final values of the interlock and  $T_{\min}$  [11]. The assessment criteria for these three indicators are generally determined by the application requirements of each company, and may vary in different industry sectors. For example, according to the standard of a world-leading car manufacturer [6], the interlock should be greater than 0.4mm for joints with aluminium alloy bottom sheet and greater than 0.2mm with a steel bottom sheet. The  $T_{\min}$  should be always greater than 0.2mm and fracture of the bottom sheet should be avoided. The rivet head height should be between 0.3mm and -0.5mm to achieve a smooth surface.

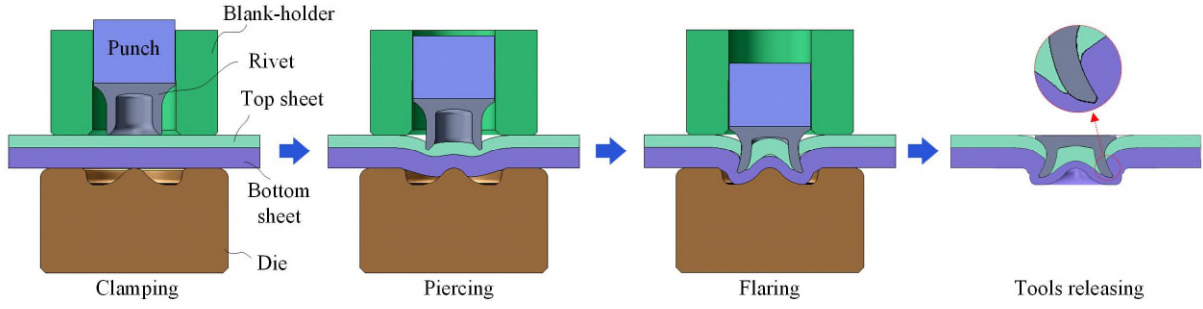


**Fig. 1** Schematic of the self-pierce riveting process

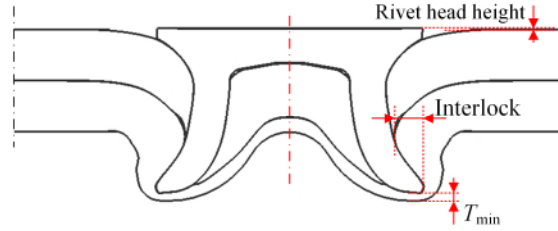


**Fig. 2** Quality evaluation indicators of the SPR joint

The SPR joint quality can be affected by many parameters, such as the sheet properties, the rivet geometry, the die profile and even the riveting speed [8][13]. For a given material combination, the selection of rivet and die is most critical for the final SPR joint quality. Many researches were carried out using experimental approach to investigate the influences of rivet and die parameters on the joint quality. For example, Xu [14] experimentally analysed the influences of the rivet length and the die geometry on the interlock and the remaining bottom sheet thickness of AA5754 SPR joints. Similarly, Ma et al. [15] investigated the effects of the rivet length and hardness, the die diameter and pip height on the rivetability of SPR joints with AA6061-T6 and mild steel CR4 sheets. Li et al. [16] evaluated the influences of the rivet tip geometry on the formation of the interlock and the  $T_{min}$  in AA5754 SPR joints. However, most of these studies focused on single-factor effects of rivet or die parameters on the SPR joint quality. In fact, during the riveting process, the rivet properties and die profile work together to affect the deformation behaviours of the rivet and sheets. Therefore, the rivet and die parameters would inevitably impose interaction effects on the final joint quality. To deepen understanding of the SPR process and facilitate the rivet and die selection, it is necessary to find out how such interaction effects affect the joint quality. Although the experimental method is a traditional and reliable approach for the study of SPR, it is not a good option to explore the interaction effects considering the heavy investments (e.g. materials, equipment and labour) and long testing time for a huge number of SPR joints.

Over the last few years, many finite element analysis (FEA) models of SPR process have been developed to predict the joint quality and assess the influences of joining parameters on the joint quality. For instance, Mucha [17] developed a two-dimensional (2D) axisymmetric SPR model in MSC Marc Mentat, and numerically evaluated the effects of the rivet material properties and the die geometries on the joint interlock and  $T_{min}$ . Han et al. [18] numerically studied the main effects of nine independent die parameters on the

interlock and the bottom sheet thickness of SPR joints with the DEFORM-2D. Jäckel et al. [19] also numerically studied the influences of five die geometrical parameters on the joint quality. FEA models are much faster than experimental SPR tests. Thus, many vehicle manufacturers gradually apply such FEA models to assist the rivet and die selection for new joints. However, for general engineers without an in depth knowledge of SPR process and FEA, running such simulation model is still a challenge and it is not easy to identify a suitable rivet and die combination. Meanwhile, the FEA model cannot provide a straightforward result to demonstrate the interaction effects between rivet and die parameters on the joint quality. Therefore, it would be a great contribution for the car industry if a fast and easy-to-use tool could be developed to predict the joint quality and to illustrate the interaction effects between the rivet and die parameters.

The regression model is a simple but effective approach to describe the relationships between independent and dependent variables. It has already been widely applied in many different industrial fields to solve real problems. For example, Bhushan [20] proposed second order regression models to study the cutting parameters' influences during the turning of aluminium alloy 7075. The power consumption and tool life were also successfully optimized by analysing the corresponding contour graphs. Singh and Ahuja [21] developed regressions models to study the influences of two swellable polymers on the bioadhesive strength and release pattern of the drug. Anawa and Olabi [22] successfully predicted the welding pool geometry of the CO<sub>2</sub> continuous laser welded joints using the proposed multiple regression models. Bitondo et al. [23] also proved the effectiveness of multiple regression models in predictions of welding force and mechanical strength of friction-stir welded aluminium joints. Zhao et al. [24] developed a stepwise regression model to predict the nugget diameter of the resistant spot welded DP600 joint with three welding parameters. Unlike the FEA simulation model, the regression model could also be used to easily visualize the interaction effects between different input variables on the target outputs by drawing contour graphs [22][23][24]. To the authors' knowledge, there are few reports on the applications of regression model or other type mathematic models in quality prediction of SPR joints.

Therefore, this study aims to develop easy-to-use regression models as an alternative to FEA model for SPR joint quality prediction and reveal the interaction effects between the rivet and die. The advantages of the FEA simulation model and orthogonal experimental design were taken to facilitate the development of the regression models and the investigation on the interaction effects. The multiple regression models were developed individually for the interlock and the  $T_{\min}$  to achieve a high prediction accuracy for each quality indicator. Experimental SPR tests were also carried out to validate the performances of the proposed models. Moreover, interaction effects between the rivet length, die depth and die diameter on SPR joint quality were systematically analysed with corresponding contour graphs drawn from the developed regression models. The importance of the Die-to-Rivet volume ration ( $R$ ) on the interaction effects was also highlighted.

## 2 Joint quality data acquisition

Before developing the mathematical prediction models, the necessary joint quality data under varying joining parameters, including the rivet length ( $L_1$ ), die diameter ( $D_1$ ) and depth ( $H_1$ ), were collected using the developed and verified FEA model. The orthogonal design method was also employed to reduce the total number of simulations.

### 2.1 FEA model of the SPR process

#### 2.1.1 Model description

The software Simufact.Forming 15, which is mainly designed for simulations of metal forming processes (e.g. forging, clinching and riveting), was adopted in this study to build up the simulation model. Fig. 3 shows the developed 2D thermal-mechanical model of the SPR process. The bottom of die was fixed while the sheet edges could move freely. A 5.3kN clamping force ( $F_1$ ) was applied on top surface of the blank-holder to clamp the two sheets together. The punch moved downward with a constant speed ( $v_1=100\text{mm/s}$ ) to press the rivet into the sheets. During the riveting process, the punch, blank-holder and die undergo very limited elastic deformation and thus were modelled as rigid bodies. While the boron steel rivet and the aluminium alloy AA5754 sheets undergo large plastic deformations and thus were modelled as elastic-plastic bodies. The mechanical properties of the boron steel rivet and the AA5754 sheets are listed in Table 1. The plastic stress-strain curves considering the temperature effect of the AA5754 were used to model the sheet deformations as shown in Fig. 4(a). The temperature change during the joining process ( $20^\circ\text{C}\sim 250^\circ\text{C}$ ) has very limited influence on the rivet properties [25], and thus only the plastic stress-strain curve at  $20^\circ\text{C}$  of the boron steel was used to model the rivet deformation as shown in Fig. 4(b).

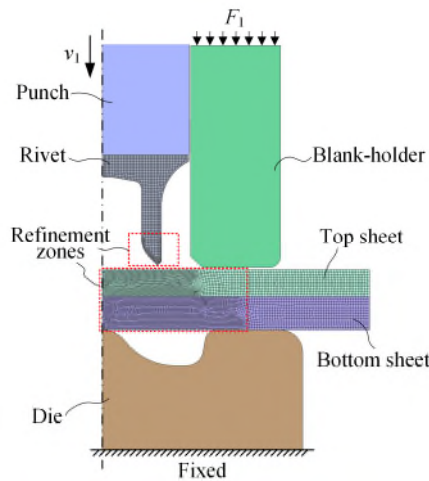
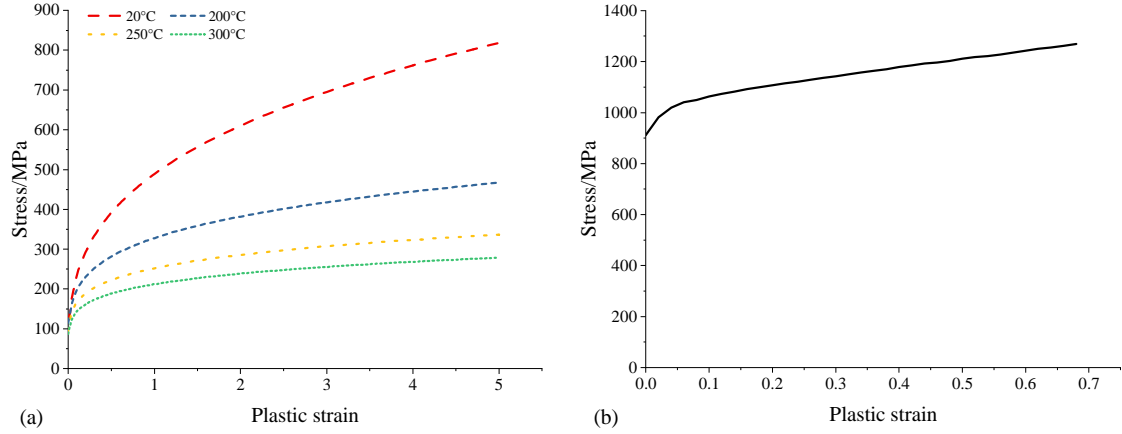


Fig. 3 Schematic of the FEA simulation model

**Table 1** Mechanical properties of the rivet [26] and sheet materials [5]

Material	Young's Modules (GPa)	Poisson's ratio	Elongation (%)	Thermal expansion coefficient (1/° C)
AA5754	70	0.33	22	2.4E-5
Boron steel	200	0.30	--	1.2E-5

**Fig. 4** Plastic stress-strain curves for (a) the AA5754 (strain rate= $1\text{s}^{-1}$ )[25] and (b) the boron steel rivet ( $20^{\circ}\text{C}$ , strain rate= $0.01\text{s}^{-1}$ )[27]

To make a balance between the simulation efficiency and accuracy, the mesh size of the rivet and the top sheet was set to 0.10mm but the mesh size of the bottom sheet was set to 0.12mm. Quad element with four gauss points was used for all the deformation parts. Automatic element re-meshing was applied on the two sheets to deal with the large material deformation during the riveting process. A geometric criterion was employed to model the top sheet separation and the critical thickness was set to 0.04mm. The Coulomb friction model was used to describe the frictions between contact parts. The friction coefficients listed in **Table 2** were identified using the inverse method. More details about the FEA simulation model can be found in the authors' previous study [27].

**Table 2** Friction coefficients between the different parts in FEA simulation model [27]

Contact pairs	Punch-Rivet	Blankholder-sheets	Rivet-Sheets	Top sheet-Bottom sheets	Bottom sheet-Die	Others
Friction coefficients	0.10	0.10	0.10	0.10	0.22	0.10

## 2.1.2 Model Validation

The capability and accuracy of the developed FEA model were verified by comparing the simulated joint quality results with the experimental SPR test results. As listed in **Table 3**, twenty-five groups of aluminium alloy AA5754 joints with different sheets, rivet and die combinations were generated using the Tucker servo SPR system shown in **Fig. 5**. Three rivets with different lengths ( $L_1$ ) (i.e. 5.0mm, 6.0mm and 6.5mm) and six dies with different diameters ( $D_1$ ) and depths ( $H_1$ ) were used in the experiments. The cross-sectional profiles

of the semi-tubular rivet and the pip die were illustrated in **Fig. 6**. The nominal rivet shank diameter and rivet hardness are Ø5.3mm and 280±30HV10 respectively. The die pip height ( $H_2$ ) is fixed at 0.0mm in all dies. The specimen size is 40mm×40mm as shown in **Fig. 7**, and at least three repetitions for each group were made. All the specimens were sectioned through the joint central axis and polished. Then, the joint cross-sectional profile was inspected using an optical microscope, and the three quality indicators (i.e. the rivet head height, the interlock and the  $T_{\min}$  shown in **Fig. 2**) were measured.

**Table 3** Joint configurations and the results for validation of the FEA model

Joint configurations					Experimental and simulation results					
Joint no.	Stack /mm (AA5754)	Rivet length $L_1$ /mm	Die		Rivet head height/mm		Interlock/mm		$T_{\min}$ /mm	
			Diameter $D_1$ /mm	Depth $H_1$ /mm	Tested (Mean)	Simulated	Tested (Mean)	Simulated	Tested (Mean)	Simulated
E1	1.0+1.8	5.0	8.0	2.0	-0.09	-0.1	0.59	0.58	0.40	0.35
E2	1.2+1.0	5.0	8.0	2.0	-0.10	-0.1	0.48	0.50	0.12	0.13
E3	1.2+1.5	5.0	8.0	2.0	-0.07	-0.1	0.51	0.52	0.33	0.31
E4	1.2+1.8	5.0	8.0	2.0	-0.10	-0.1	0.53	0.51	0.53	0.48
E5	1.2+2.0	5.0	8.0	2.0	-0.09	-0.1	0.52	0.55	0.72	0.72
E6	1.2+1.8	6.0	8.0	2.0	-0.14	-0.1	0.86	0.73	0.24	0.26
E7	1.5+1.5	5.0	9.0	1.6	0.00	0.0	0.42	0.38	0.53	0.51
E8	1.2+1.8	5.0	9.0	1.6	-0.11	-0.1	0.59	0.60	0.47	0.46
E9	1.2+2.0	6.0	9.0	1.6	0.05	0.0	0.94	0.85	0.38	0.30
E10	1.8+2.0	6.0	9.0	1.6	0.08	-0.1	0.70	0.67	0.67	0.74
E11	2.5+2.0	6.0	9.0	1.6	0.10	-0.1	0.31	0.35	0.93	0.90
E12	1.2+1.2	5.0	10.0	1.8	-0.08	-0.1	0.36	0.32	0.24	0.28
E13	1.2+1.8	5.0	10.0	1.8	-0.07	-0.1	0.48	0.47	0.48	0.50
E14	1.8+1.2	5.0	10.0	1.8	-0.07	-0.1	0.13	0.13	0.63	0.63
E15	1.8+1.8	5.0	10.0	1.8	-0.11	-0.1	0.30	0.25	1.26	1.04
E16	1.0+1.8	5.0	10.0	2.0	-0.04	-0.1	0.49	0.51	0.44	0.37
E17	1.2+1.5	5.0	10.0	2.0	-0.03	-0.1	0.34	0.36	0.40	0.36
E18	1.2+1.8	5.0	10.0	2.0	-0.04	-0.1	0.47	0.44	0.62	0.53
E19	1.2+2.0	5.0	10.0	2.0	-0.06	-0.1	0.49	0.46	0.67	0.69
E20	1.5+1.8	5.0	10.0	2.0	-0.05	-0.1	0.33	0.31	0.85	0.77
E21	2.0+1.8	5.0	10.0	2.0	-0.03	-0.1	0.18	0.19	1.24	1.25
E22	1.2+1.8	6.0	10.0	2.0	-0.13	-0.1	0.90	0.84	0.28	0.24
E23	1.2+1.8	6.5	10.0	2.0	-0.09	-0.1	1.20	1.05	0.22	0.14
E24	1.2+1.8	5.0	11.0	1.8	-0.07	-0.1	0.36	0.37	0.56	0.52
E25	1.2+1.8	5.0	11.0	2.0	-0.02	-0.1	0.40	0.35	0.60	0.58



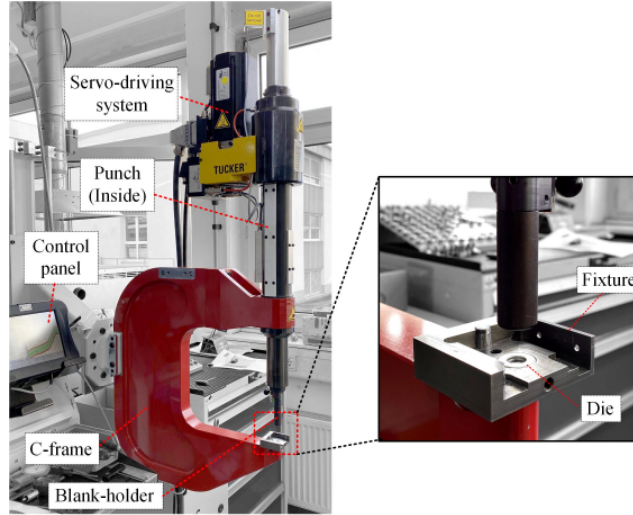


**Fig. 5** Structure of the Tucker SPR system

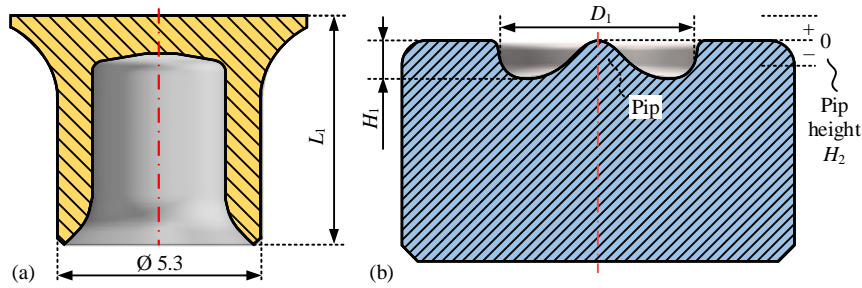


**Fig. 6** Schematics of (a) the semi-tubular rivet and (b) the pip die

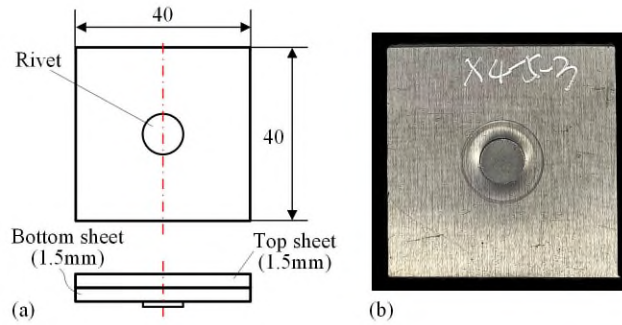


**Fig. 7** Dimensions of the SPR specimen

The twenty-five SPR joints were also simulated with the developed FEA model. The magnitude of the rivet head height is highly associated with the final values of the interlock and  $T_{\min}$  [6]. To properly evaluate the prediction accuracy of the FEA model, the measured rivet head height from the experimental test (listed in **Table 3**) was implemented as the termination criterion of the corresponding SPR simulation. The simulated joint cross-sectional profile, interlock and  $T_{\min}$  were also recorded for each joint.

The joint cross-sectional profiles from the experimental tests and the FEA model are given in **Fig. 8**. For easier comparisons, half of the simulated joint profiles were superimposed on the tested ones. It can be identified that there are no gross differences between the simulated and experimental joint profiles. The local

material deformation of the bottom sheet (e.g. Zone1 and Zone2) and the gaps between the rivet and top sheet (e.g. Zone3 and Zone4) were successfully captured by the FEA model. To quantitatively evaluate the prediction accuracy of the FEA model, the bottom sheet thickness at the joint centre ( $T_c$ ), the horizontal bottom sheet thickness beside the rivet tip ( $T_h$ ) and the deformed rivet shank radius ( $R_f$ ) were measured on the tested and simulated profiles shown in **Fig. 8**. Comparisons between the simulated and the tested three indicators are given in **Fig. 9**. The calculated mean absolute errors (MAE) between the simulation and experimental results for the  $T_c$ ,  $R_f$  and  $T_h$  were 0.060mm, 0.073mm and 0.066mm respectively. The calculated mean absolute percentage errors (MAPE) for the  $T_c$ ,  $R_f$  and  $T_h$  were 13.59%, 1.94% and 10.64% respectively. Therefore, it can be concluded that the developed FEA model has the capability to predict the joint cross-sectional profile. The average values of the interlock and the  $T_{\min}$  obtained from the simulated and the tested joints are listed in **Table 3** and illustrated in **Fig. 10**. The calculated MAE between the simulation and experimental results for the interlock and the  $T_{\min}$  were 0.037mm and 0.045mm respectively, and the corresponding MAPE were 6.75% and 9.53%. The Pearson's correlation coefficient ( $r$ ) between the experimental and simulation results was also calculated. The calculated  $r$  for the interlock and the  $T_{\min}$  were 0.988 and 0.981 respectively. **Therefore**, the interlock and  $T_{\min}$  values were accurately predicted by the FEA simulation model.

From the analysis and comparisons above, it is reasonable to confirm that the developed FEA model is capable of predicting the quality and material deformation of SPR joints (boron steel rivet + AA5754 sheets) with varying rivet and die profiles.

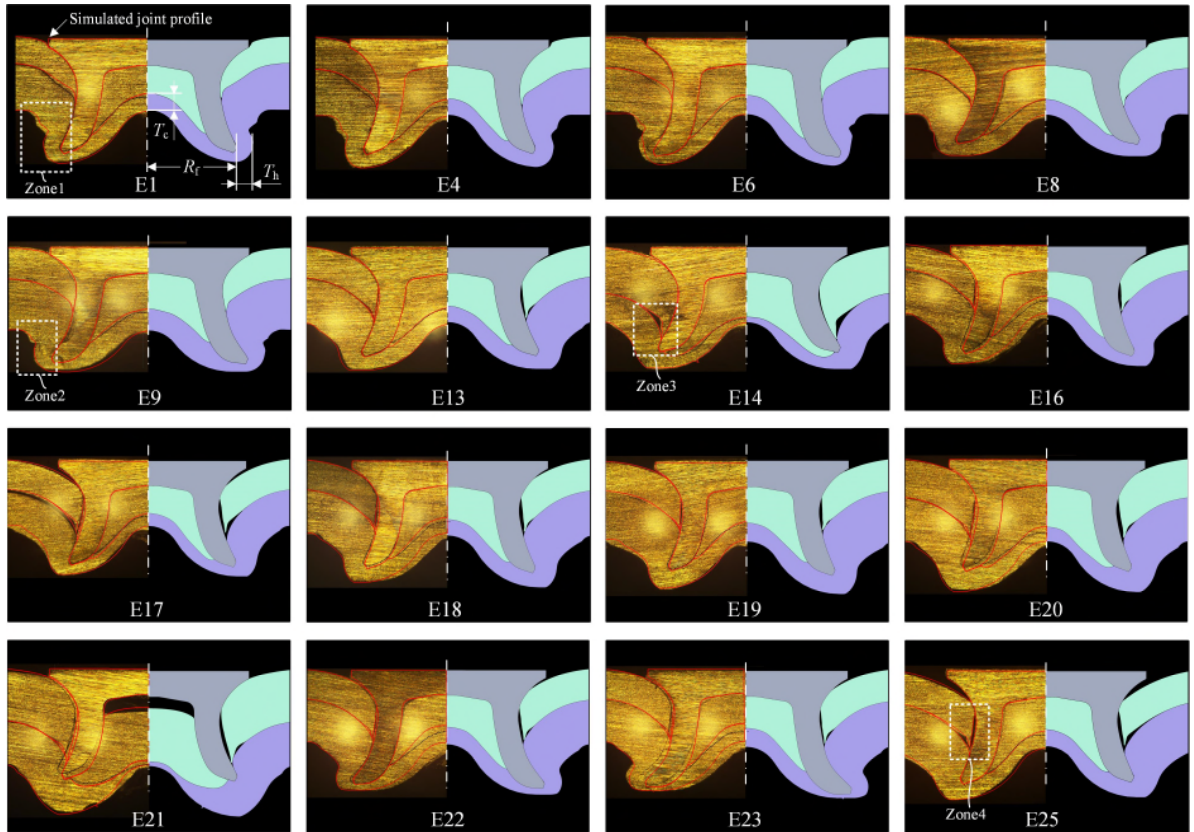


**Fig. 8** Comparisons of the joint cross-sectional profiles from the experimental tests and FEA simulations

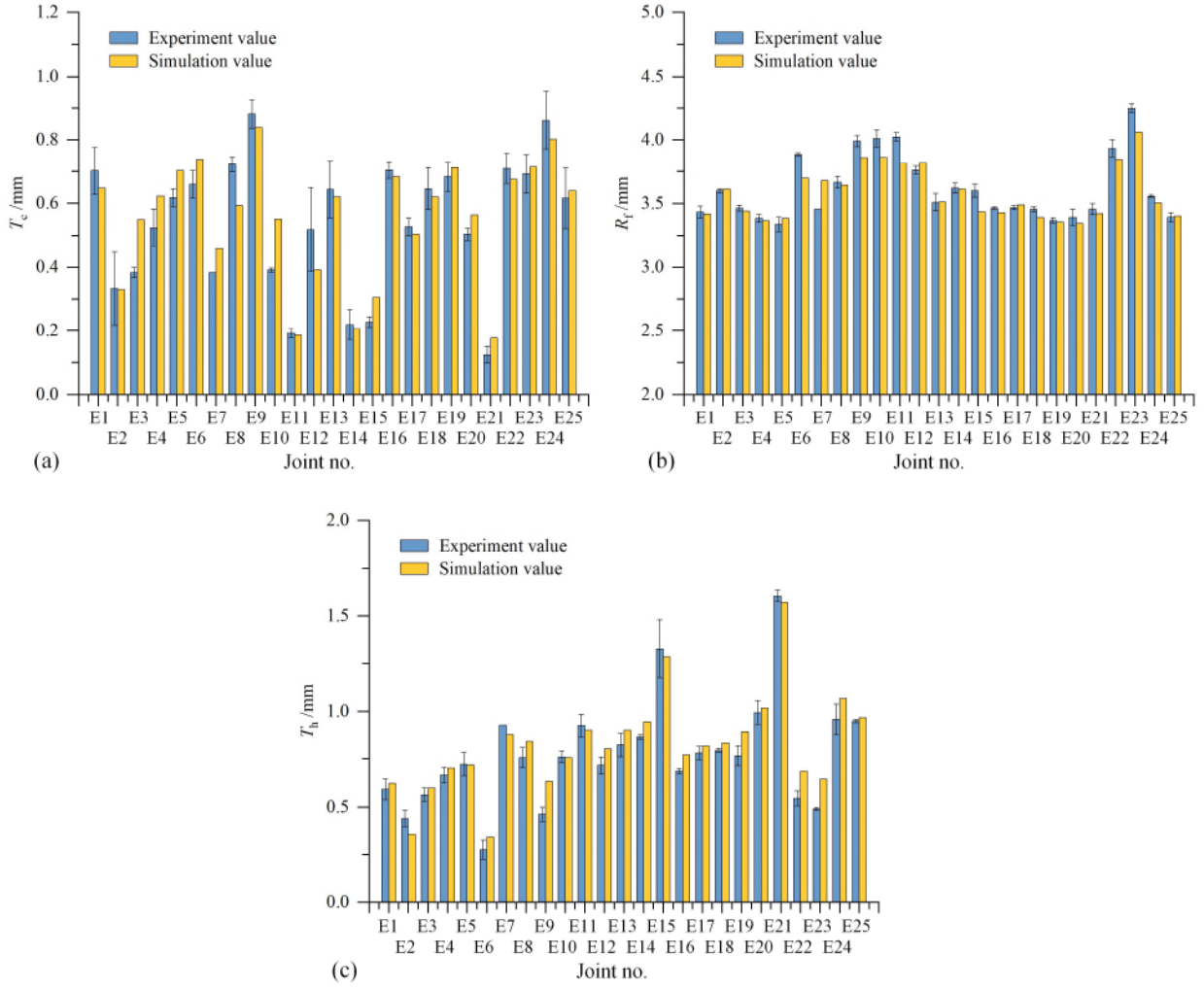


**Fig. 9** Comparisons of (a) the  $T_c$ , (b) the  $R_f$  and (c) the  $T_h$  from experimental tests and FEA simulations

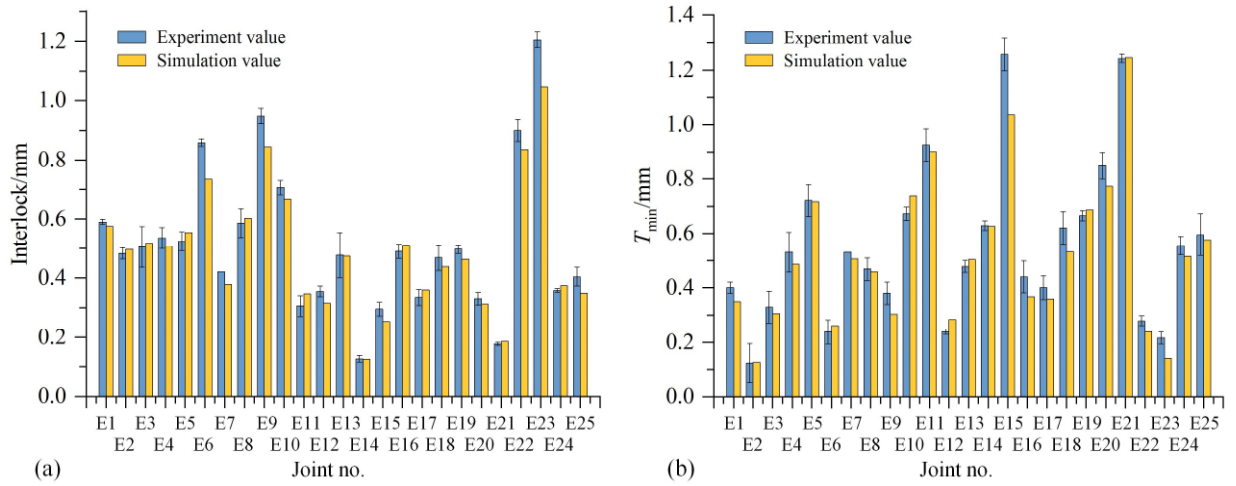


**Fig. 10** Comparisons of (a) the interlock and (b) the  $T_{min}$  from experimental tests and FEA simulations

## 2.2 Orthogonal test

When collecting the joint quality data for further mathematical model development, the orthogonal design method was adopted to minimize the total number of SPR simulations required. The rivet length ( $L_1$ ), die diameter ( $D_1$ ) and depth ( $H_1$ ) are the three independent variables, and each independent variable has three levels as listed in **Table 4**. The hardness of the Ø5.3mm boron steel rivets is  $280 \pm 30\text{HV}_{10}$ . The die geometries are modified based on the reference die in **Fig. 11** ( $D_1=9.0\text{mm}$ ,  $H_1=1.6\text{mm}$ ,  $H_2=0.0\text{mm}$ ). Moreover, to investigate the interaction effects of the  $L_1$ ,  $D_1$  and  $H_1$  on the joint quality, the interaction terms ( $L_1 \times D_1$ ,  $L_1 \times H_1$  and  $D_1 \times H_1$ ) between these independent variables were also considered in the orthogonal test. According to the number of independent variables, interaction terms and levels, the  $L_{27} (3^{13})$  orthogonal table with 13 columns and 27 rows was selected (**Table 5**). Four null columns were left and treated as error terms.

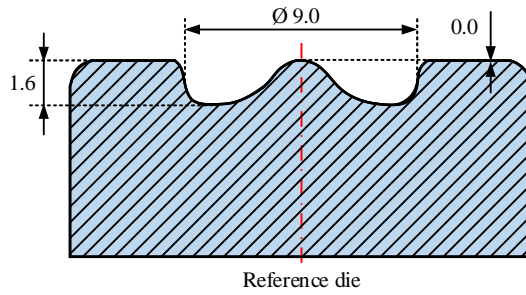


**Fig. 11** Dimonsions of the reference pip die

**Table 4** Independent variables and levels of the orthogonal test

Level	Rivet length $L_1/\text{mm}$	Die diameter $D_1/\text{mm}$	Die depth $H_1/\text{mm}$
1	5	8.0	1.6
2	6	9.0	1.8
3	6.5	10.0	2.0

All the 27 SPR joints with different configurations in **Table 5** were made using the developed FEA simulation model. For consistency, all the simulations were terminated when the rivet head height reached to 0.0mm. By observing all the 27 simulated joint cross-sectional profiles, it was found that the  $T_{\min}$  appeared around the rivet tip in most of the joints. Therefore, to keep the data uniformity and make it easier for the mathematical prediction model development, the minimum bottom sheet thickness around the rivet tip in all the 27 joints was measured as the  $T_{\min}$  in this study. **Table 5** shows the simulated values of interlock and  $T_{\min}$  for the 27 SPR joints.

**Table 5**  $L_{27}$  ( $3^{13}$ ) orthogonal test design and simulation results

Joint No.	Variables and levels													Simulation results	
	$L_1$	$D_1$	$(L_1 \times D_1)_1$	$(L_1 \times D_1)_2$	$H_1$	$(L_1 \times H_1)_1$	$(L_1 \times H_1)_2$	$(D_1 \times H_1)_1$	Null	Null	$(D_1 \times H_1)_2$	Null	Null	Interlock /mm	$T_{\min}$ /mm
S-1	1	1	1	1	1	1	1	1	1	1	1	1	1	0.37	0.56
S-2	1	1	1	1	2	2	2	2	2	2	2	2	2	0.39	0.55
S-3	1	1	1	1	3	3	3	3	3	3	3	3	3	0.35	0.52
S-4	1	2	2	2	1	1	1	2	2	2	3	3	3	0.38	0.51
S-5	1	2	2	2	2	2	2	3	3	3	1	1	1	0.33	0.50
S-6	1	2	2	2	3	3	3	1	1	1	2	2	2	0.27	0.52
S-7	1	3	3	3	1	1	1	3	3	3	2	2	2	0.28	0.56
S-8	1	3	3	3	2	2	2	1	1	1	3	3	3	0.24	0.57
S-9	1	3	3	3	3	3	3	2	2	2	1	1	1	0.20	0.59
S-10	2	1	2	3	1	2	3	1	2	3	1	2	3	0.57	0.26
S-11	2	1	2	3	2	3	1	2	3	1	2	3	1	0.60	0.32
S-12	2	1	2	3	3	1	2	3	1	2	3	1	2	0.61	0.34
S-13	2	2	3	1	1	2	3	2	3	1	3	1	2	0.74	0.26
S-14	2	2	3	1	2	3	1	3	1	2	1	2	3	0.71	0.27
S-15	2	2	3	1	3	1	2	1	2	3	2	3	1	0.70	0.25
S-16	2	3	1	2	1	2	3	3	1	2	2	3	1	0.59	0.27
S-17	2	3	1	2	2	3	1	1	2	3	3	1	2	0.55	0.28
S-18	2	3	1	2	3	1	2	2	3	1	1	2	3	0.52	0.25
S-19	3	1	3	2	1	3	2	1	3	2	1	3	2	0.62	0.16
S-20	3	1	3	2	2	1	3	2	1	3	2	1	3	0.66	0.20
S-21	3	1	3	2	3	2	1	3	2	1	3	2	1	0.69	0.24
S-22	3	2	1	3	1	3	2	2	1	3	3	2	1	0.89	0.23
S-23	3	2	1	3	2	1	3	3	2	1	1	3	2	0.88	0.23
S-24	3	2	1	3	3	2	1	1	3	2	2	1	3	0.86	0.20
S-25	3	3	2	1	1	3	2	3	2	1	2	1	3	0.75	0.26
S-26	3	3	2	1	2	1	3	1	3	2	3	2	1	0.75	0.19
S-27	3	3	2	1	3	2	1	2	1	3	1	3	2	0.72	0.18

### 3 Mathematic prediction models for the interlock and the $T_{\min}$

#### 3.1 Analysis of variance (ANOVA)

The analysis of variance (ANOVA) was performed using the orthogonal test results to evaluate the significances of the three independent variables ( $L_1$ ,  $D_1$  and  $H_1$ ) and their interaction terms ( $L_1 \times D_1$ ,  $L_1 \times H_1$  and  $D_1 \times H_1$ ) on the interlock and the  $T_{\min}$  with software Minitab 19. **Table 6** and **Table 7** list the results of the ANOVA for the interlock and the  $T_{\min}$  respectively. In general, the smaller the p-value is, the more significant the variable is. The influence of a variable on the response is considered as significant if the corresponding p-value is smaller than 0.05 or 0.10, depending on the **selected** significant level (0.05 or 0.10). It was apparent that all the three independent variables and their interaction terms had significant influences on the interlock as the p-values were less than 0.05. However, under the studied joint configurations, the rivet length ( $L_1$ ) showed a significant influence on the  $T_{\min}$ , whilst the other two independent variables ( $D_1$

and  $H_1$ ) and the three interaction terms ( $L_1 \times D_1$ ,  $L_1 \times H_1$  and  $D_1 \times H_1$ ) did not show remarkable effect on the  $T_{\min}$ .

**Table 6** Results of ANOVA for the interlock

Source	DF	Adj SS	Adj MS	F-Value	p-Value
$L_1$	2	0.93608	0.468041	4322.59	0.000
$D_1$	2	0.08224	0.041120	379.77	0.000
$L_1 \times D_1$	4	0.06324	0.01581	146.00	0.000
$H_1$	2	0.00424	0.002121	19.59	0.001
$L_1 \times H_1$	4	0.00465	0.001163	10.74	0.003
$D_1 \times H_1$	4	0.00937	0.00234	21.64	0.000
Error	8	0.00087	0.000108	--	--
Total	26	1.10069	--	--	--

**Table 7** Results of ANOVA for the  $T_{\min}$

Source	DF	Adj SS	Adj MS	F-Value	P-Value
$L_1$	2	0.561094	0.280547	266.93	0.000
$D_1$	2	0.002480	0.001240	1.18	0.356
$L_1 \times D_1$	4	0.00833	0.00208	1.98	0.191
$H_1$	2	0.000168	0.000084	0.08	0.924
$L_1 \times H_1$	4	0.00071	0.00018	0.17	0.948
$D_1 \times H_1$	4	0.00324	0.00081	0.77	0.574
Error	8	0.008408	0.001051	--	--
Total	26	0.584434	--	--	--

### 3.2 Development of the regression models

Multiple regression analysis was carried out using the software Minitab 19 to develop the prediction models for the interlock and  $T_{\min}$ . According to the results of ANOVA, the three independent variables and the three interaction terms were significant for the interlock. So all of them were included in the multiple regression model of interlock in Eq. (1). As for the  $T_{\min}$ , although only the rivet length was a statistically significant variable under the studied joint configurations, the influences of other variables on the  $T_{\min}$  were also considered in this study. Therefore, all of them were also involved in the regression model of  $T_{\min}$  in Eq. (2).

$$Interlock = \alpha_0 + \alpha_1 L_1 + \alpha_2 D_1 + \alpha_3 H_1 + \alpha_4 L_1 \times D_1 + \alpha_5 L_1 \times H_1 + \alpha_6 D_1 \times H_1 \quad (1)$$

$$T_{\min} = \beta_0 + \beta_1 L_1 + \beta_2 D_1 + \beta_3 H_1 + \beta_4 L_1 \cdot D_1 + \beta_5 L_1 \cdot H_1 + \beta_6 D_1 \cdot H_1 \quad (2)$$

The unknown coefficients in the regression models (the  $\alpha_0$  to  $\alpha_6$ , and the  $\beta_0$  to  $\beta_6$ ) were identified with the orthogonal test results by the software Minitab 19. The final regression models of interlock and  $T_{\min}$  are shown in Eq. (3). and Eq. (4).

$$Interlock = 2.030 - 0.543L_1 - 0.196D_1 + 0.280H_1 + 0.069L_1 \cdot D_1 + 0.125L_1 \cdot H_1 - 0.120D_1 \cdot H_1 \quad (3)$$

$$T_{\min} = -0.360 - 0.093L_1 + 0.206D_1 + 0.793H_1 - 0.012L_1 \cdot D_1 - 0.016L_1 \cdot H_1 - 0.076D_1 \cdot H_1 \quad (4)$$

### 3.3 Evaluation of the regression models

The fitting accuracy of the regression model was evaluated statistically by five indicators. The coefficient of determination ( $R^2$ ) describes how close the predicted and the actual values lie, and the  $R^2$  close to 1 indicates the good fitting achieved using this regression model. The adjusted  $R^2$  ( $R^2_{adj}$ ), which is effective at eliminating the influence of the independent variables' numbers, was also used to evaluate the accuracy of the regression models. Meanwhile, the prediction  $R^2$  ( $R^2_{pred}$ ), the mean absolute error (MAE) and the standard error (S), were also employed to further assess the model accuracy. The evaluation results for the regression models of interlock and  $T_{min}$  are listed in Table 8. Both of the  $R^2$  and  $R^2_{adj}$  for the interlock were over 0.860, and the value of the  $R^2_{pred}$  was up to 0.828. The corresponding MAE and S values for the interlock were 0.055mm and 0.076mm. For the  $T_{min}$ , the  $R^2$ ,  $R^2_{adj}$  and  $R^2_{pred}$  were as high as 0.949, 0.934 and 0.885 respectively. The corresponding MAE and S values were 0.029mm and 0.039mm. Therefore, the developed regression models are accurate enough to predict the interlock and the  $T_{min}$ . In other words, it is proved that the developed multiple regression models could be used to replace this FEA simulation model for the SPR joint quality prediction under the studied joint configurations.

**Table 8** Evaluation results of the regression models for the interlock and  $T_{min}$

	$R^2$	$R^2_{adj}$	$R^2_{pred}$	MAE/mm	S/mm
Interlock	0.896	0.865	0.828	0.055	0.076
$T_{min}$	0.949	0.934	0.885	0.029	0.039

### 3.4 Validation of the regression models

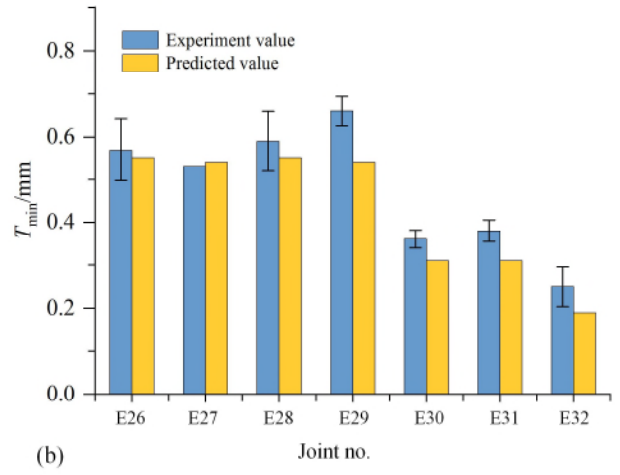
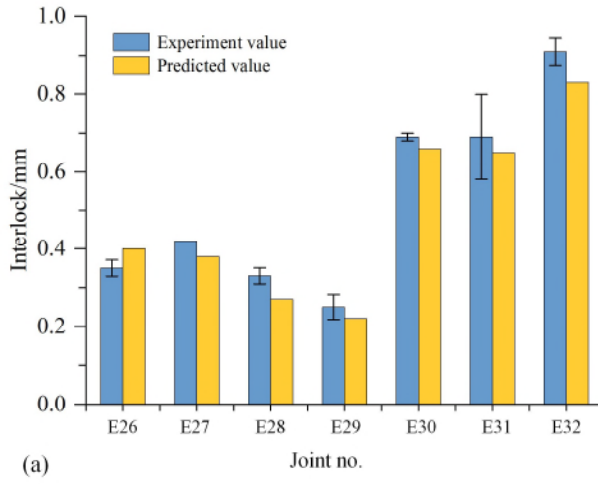
To verify the performance of the developed regression models in real applications, seven groups of SPR joints with different rivets and dies, as shown in Table 9, were made using laboratory experimental tests. Three repetitions for each group were performed. The average values of the interlock and the  $T_{min}$  from the experimental SPR tests and the predicted values from the regression models are recorded in Table 9 and compared graphically in Fig. 12. The calculated MAE between the predicted and experimental results for the interlock and the  $T_{min}$  were 0.047mm and 0.053mm respectively, and the corresponding MAPE were 10.4% and 12.3%. The calculated Pearson's correlation coefficient ( $r$ ) for the interlock and  $T_{min}$  were 0.987 and 0.964 respectively. Thus, the predicted interlock and  $T_{min}$  matched well with the experimental results. This also indicated the high prediction accuracy of the developed regression models for the interlock and the  $T_{min}$ .

According to the statistic evaluation and experimental verification results, it is reasonable to conclude that the developed multiple regression models are effective for quality prediction of the studied SPR joints. Meanwhile, the model development method used in this study is also proved to be valid.



**Table 9** Joint configurations and the results for the validation of the regression models

Joint configurations					Experimental and predicted results					
Joint no.	Stack /mm (AA5754)	Rivet length $L_1$ /mm	Die		Rivet head height/mm		Interlock/mm		$T_{min}$ /mm	
			Diameter $D_1$ /mm	Depth $H_1$ /mm	Tested (Mean)	Predicted	Tested (Mean)	Predicted	Tested (Mean)	Predicted
E26	1.5+1.5	5.0	8.0	2.0	-0.04	0	0.35	0.40	0.57	0.55
E27		5.0	9.0	1.6	0.02	0	0.42	0.38	0.53	0.54
E28		5.0	10.0	1.8	-0.07	0	0.33	0.27	0.59	0.55
E29		5.0	10.0	2.0	-0.05	0	0.25	0.22	0.66	0.54
E30		6.0	9.0	1.6	0.02	0	0.69	0.66	0.36	0.31
E31		6.0	10.0	1.8	-0.05	0	0.69	0.65	0.38	0.31
E32		6.5	10.0	1.8	-0.06	0	0.91	0.83	0.25	0.19

**Fig. 12** Comparisons between the experimental values and the predicted values using the regression models: (a) the interlock and (b) the  $T_{min}$ 

#### 4 Interaction analysis between the rivet and die parameters on the interlock and the $T_{min}$

Unlike the experimental SPR test or the FEA simulation model, the interaction effects between different joining parameters on the joint quality can be easily inspected by observing the contour graphs drawn from the developed regression models. In this section, the interaction effects between the rivet and die parameters ( $L_1$ ,  $D_1$  and  $H_1$ ) on the interlock and the  $T_{min}$  were systematically analysed. Some simulated joint cross-sectional profiles are also presented to further verify the contour graphs and to explain the changing trends of the interlock and the  $T_{min}$ . All the discussions were carried out on the basis of a uniform rivet head height (0.0mm). To avoid repetition, **not all** representative contour graphs and interaction effects were presented and discussed in detail.



#### 4.1 Interaction effects between the $L_1$ and $D_1$

When the die depth ( $H_1$ ) was fixed at 1.8mm, the contour graphs of the interlock and the  $T_{\min}$  with varying rivet length ( $L_1$ ) and die diameter ( $D_1$ ) are plotted in **Fig. 13**. Apparent interaction effects between the rivet length and die diameter on the interlock were indicated by the non-parallel lines shown in **Fig. 13(a)**. With the die diameter increased from 8.0mm to 10.0mm, the interlock demonstrated a decreasing trend when the rivet length was smaller than 6.0mm, but an increasing tendency when the rivet length was greater than 6.0mm. With the rivet length increased from 5.0mm to 6.5mm, a higher increasing rate (a larger gradient density) of the interlock was observed when the die had a larger diameter. In contrast, **very weak interaction effects on the  $T_{\min}$  were found because of the almost parallel contour lines in Fig. 13(b)**. When the die diameter increased from 8.0mm to 10.0mm, the  $T_{\min}$  kept almost constant with different rivet lengths. While when the rivet length increased from 5.0mm to 6.5mm, the  $T_{\min}$  rapidly decreased at almost the same rate with different die diameters. The rivet length almost dominated the magnitude of the  $T_{\min}$ , which is in agreement with the ANOVA results in **Table 7**.

To assist the contour graph analysis, the simulated joint cross-sectional profiles at the points a~i in **Fig. 13** are presented in **Fig. 14**. In both figures, the interlock showed an increasing trend as the rivet length increased, but irregular changes when the die diameter varied. In contrast, the  $T_{\min}$  decreased as the rivet length increased, but remained almost constant as the die diameter increased. A good agreement between the predicted results from the developed regression models and the FEA simulation model was found, except for the interlock values in **Fig. 14** (e) and (f) underestimated by the regression model. This might be attributed to the inherent limitation of the adopted regression model, which could only describe a monotonous growth or decline trend.

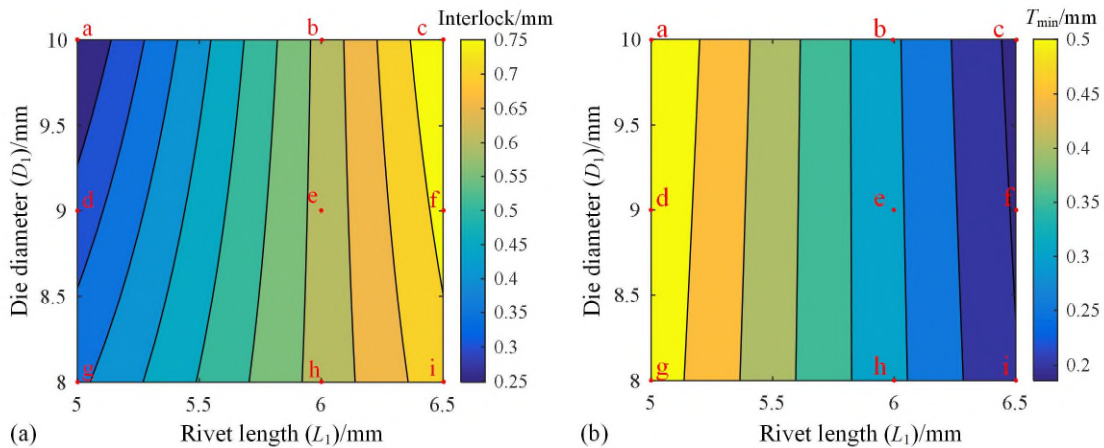


**Fig. 13** Contour graphs of (a) the interlock and (b) the  $T_{\min}$  with different rivet lengths and die diameters (Die depth=1.8mm)

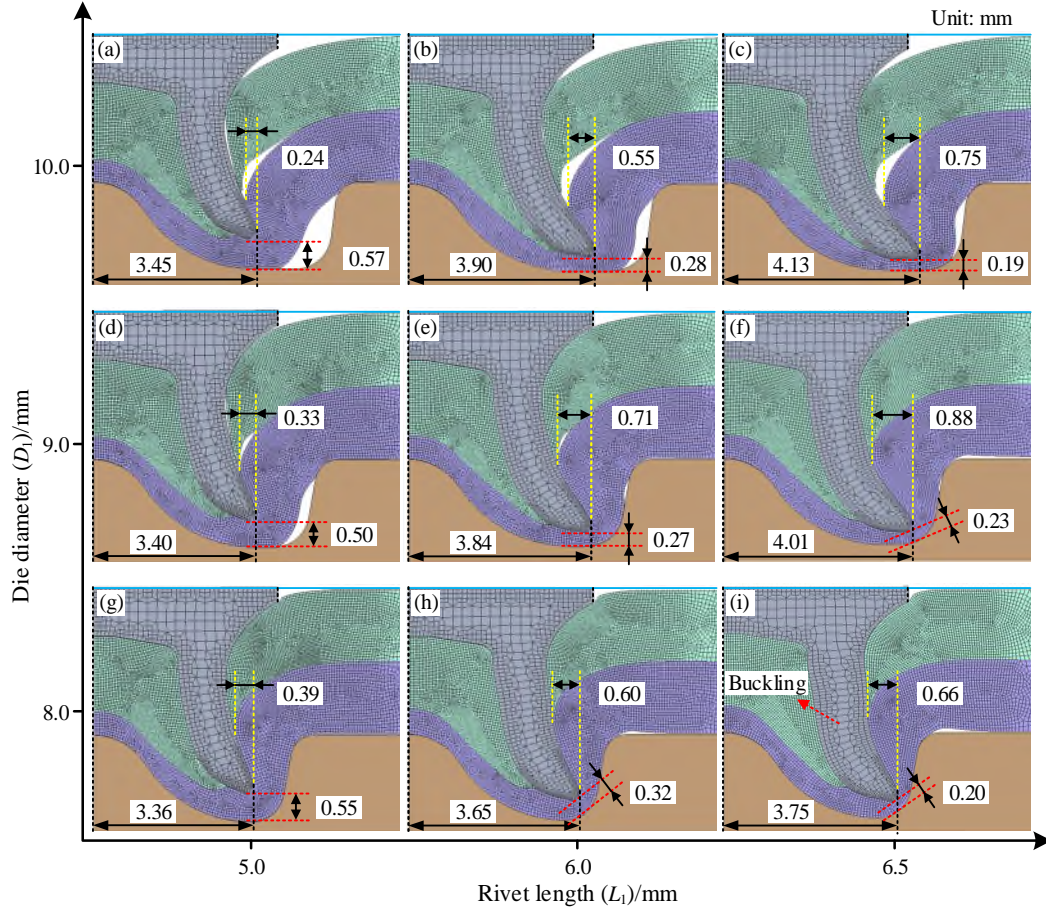


**Fig. 14** Simulated joint cross-sectional profiles with different rivet lengths and die diameters (Die depth=1.8mm)

Such interaction effects between the rivet and die parameters on the interlock are attributed directly to the deformation behaviour of the rivet and the sheets. As key components in the SPR process, the rivet is used to pierce through the top sheet and flare into the bottom sheet. **The specially designed die is used** to guide the rivet flaring and the sheet deforming into its cavity. **To** achieve a sound SPR joint with a flush head height (approx. 0.0mm), **the rivet volume ( $V_r$ ) should be equal to the die cavity volume ( $V_d$ ) or slightly larger if considering the rivet and sheet material compressions**, as shown in **Fig. 15**. **Table 10** lists the volumes of the rivets and the dies used in this study. In practice, if the  $V_d$  was much smaller than the  $V_r$ , as shown in **Fig. 16** (a), the die cavity could not accommodate all the material pressed into it. Once the die cavity was fully filled, the die would provide a high resistance force to prevent further downward movement of the rivet. This would lead to buckling of the rivet shank, and impose negative effects on the interlock formation. In contrast, if the  $V_d$  became much larger than the  $V_r$  by increasing the die diameter ( $D_1$ ) as shown in the **Fig. 16** (b), there would be always a void space underneath the bottom sheet. So, the bottom sheet became easier to be deformed into the die cavity and imposed less resistance force on the outer surface of the rivet shank ( $F_{out}$ ). While the resistance force applied on the inner surface of the rivet shank ( $F_{in}$ ) kept almost unchanged considering the similar filling conditions of the rivet cavity. As a result, the rivet shank flared a larger distance, but **was not effectively inserted into** the bottom sheet to form the interlock. Therefore, the

maximum interlock value would be always achieved when the  $V_d$  was close to the  $V_r$ , in which the rivet shank **could be** inserted effectively into the bottom sheet to form the interlock without buckling.

When the die diameter increased from 8.0mm to 10.0mm, due to the different initial Die-to-Rivet volume ratios ( $R=V_d/V_r$ ), the interlock demonstrated different changing trends at 5.0mm, 6.0mm and 6.5mm rivet lengths. For the 5.0mm long rivets, the values of the  $R$  in **Fig. 14** (g), (d) and (a) were 0.88, 1.14 and 1.44 respectively, which resulted in a rapid decrease of the interlock from 0.39mm to 0.24mm. While for the 6.0mm and 6.5mm rivets, severe rivet shank buckling was observed in **Fig. 14** (h) and (i) due to the small values of the  $R$  (0.77 and 0.73). With the increment of the die diameter, the reduction of the rivet shank buckling imposed a positive effect on the interlock formation in **Fig. 14** (e) and (f), but then the interlock decreased when the  $R$  became much larger (i.e. 1.26 in **Fig. 14**(b) and 1.19 in **Fig. 14**(c)). Thus, with the 6.0mm and 6.5mm rivets, the interlock first increased but then decreased as the die diameter increased.

When the rivet length increased from 5.0mm to 6.5mm, the interlock had a smaller increasing speed with the 8.0mm die diameter shown in **Fig. 14**. **This is because the rivet shank underwent more and more severe buckling with the reduction of the  $R$  value.**

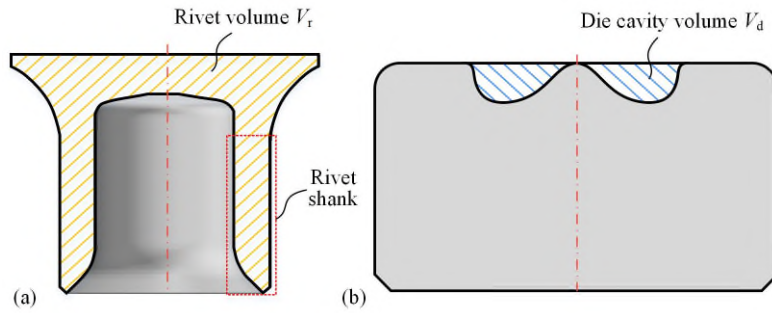


**Fig. 15** Schematic of (a) the rivet volume  $V_r$  and (b) the die cavity volume  $V_d$

**Table 10** Rivet volumes and die cavity volumes

Rivet		Die		
Length $L_1/\text{mm}$	Volume $V_r/\text{mm}^3$	Diameter $D_1/\text{mm}$	Depth $H_1/\text{mm}$	Volume $V_d/\text{mm}^3$
5.0	90.0	8.0	1.6	70.07
			1.8	79.54
			2.0	89.07
6.0	102.3	9.0	1.6	91.58
			1.8	103.02
			2.0	111.03
6.5	108.6	10.0	1.6	116.21
			1.8	129.26
			2.0	142.84

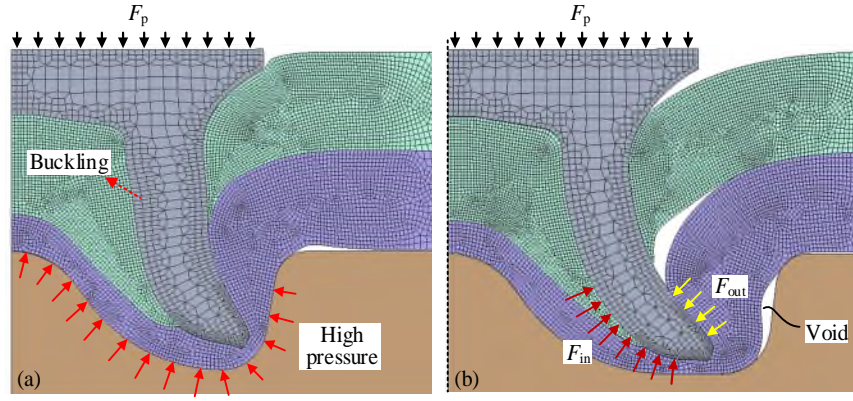


**Fig. 16** Joint cross-sectional profiles with (a)  $V_d < V_r$  and (b)  $V_d > V_r$  during the SPR processes

## 4.2 Interaction effects between the $L_1$ and $H_1$

**Fig. 17** shows the contour graphs of the interlock and the  $T_{min}$  with different rivet lengths ( $L_1$ ) and die depths ( $H_1$ ) when the die diameter ( $D_1$ ) was fixed at 9.0mm. As shown in **Fig. 17** (a), significant interaction effects indicated by the non-parallel lines were also found on the interlock. When the die depth increased from 1.6mm to 2.0mm, the interlock showed a decreasing trend and its reducing speed slowly decreased as the rivet length increasing from 5.0mm to 6.0mm. Once the rivet length **became** greater than 6.0mm, the interlock **remained** almost constant with the increment of the die depth. In contrast, the parallel lines shown in **Fig. 17** (b) indicated the very weak interaction effects on the  $T_{min}$ . The rivet length showed a dominant influence on the value of the  $T_{min}$ , while the die depth **demonstrated** little effect on the  $T_{min}$  under the studied joint configurations. The simulated joint cross-sectional profiles at points a~i in **Fig. 17** are presented in **Fig. 18**. **It can be seen from these two figures that** the predicted joint quality by the developed regression models matched well with that from the FEA simulation model. For a given die depth, the interlock increased but  $T_{min}$  decreased as the rivet length increased. For a given rivet length, **the interlock decreased but the  $T_{min}$  remained almost unchanged** as the die depth increased.

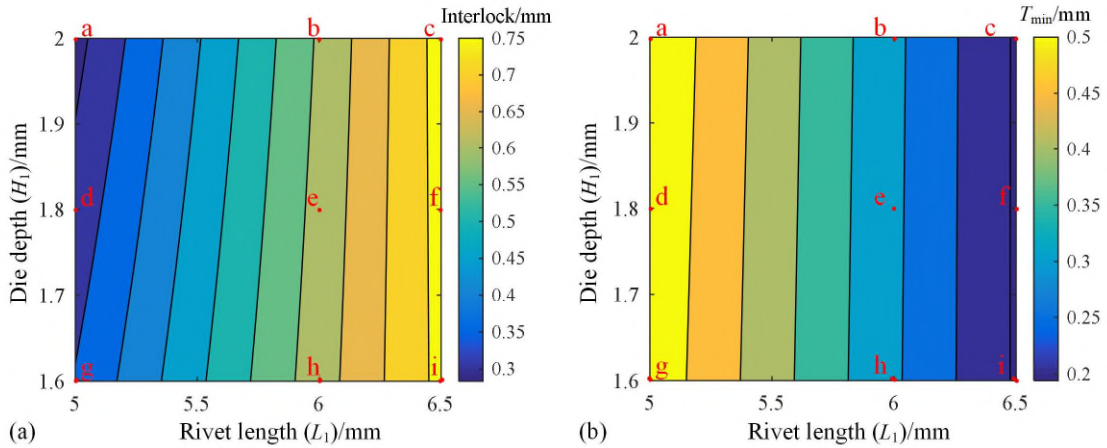


**Fig. 17** Contour graphs of (a) the interlock and (b) the  $T_{min}$  with different rivet lengths and die depths (Die diameter=9.0mm)



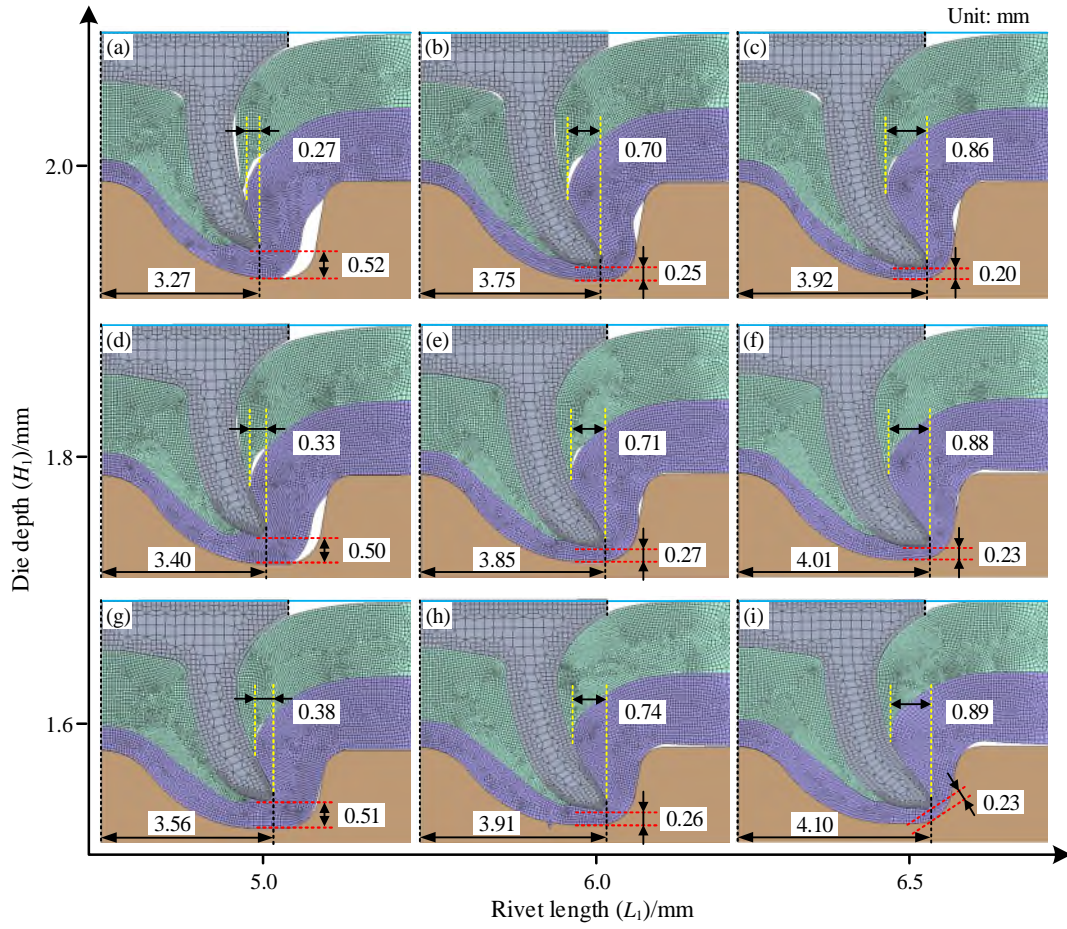


**Fig. 18** Simulated joint cross-sectional profiles with different rivet lengths and die depth (Die diameter=9.0mm)

The increment of die depth could also increase the  $V_d$  and result in a larger Die-to-Rivet volume ratio ( $R$ ). While different from the die diameter, a larger die depth could lead to an easier downward movement of the bottom sheet. As a result, the rivet shank flared less and a smaller interlock was formed. Such effect was more significant for the 5.0mm long rivets than the 6.0mm and 6.5mm rivets: the interlock showed a larger decrease with the 5.0mm long rivets, but reduced a smaller value with the 6.0mm and 6.5mm rivets because of the reduction of the rivet shank buckling degrees in **Fig. 18** (e) and (f).

### 4.3 Interaction effects between the $D_1$ and $H_1$

When the rivet length ( $L_1$ ) was fixed at 5.0mm, the contour graphs of the interlock and the  $T_{\min}$  with different die diameters ( $D_1$ ) and depths ( $H_1$ ) are shown in **Fig. 19**. Significant interaction effects were indicated by the non-parallel lines on the interlock, as shown in **Fig. 19** (a). When the die depth increased from 1.6mm to 2.0mm, the interlock decreased at a slower speed with a small diameter die (e.g.  $D_1=8.0$ mm) than with a larger one (e.g.  $D_1=10.0$ mm). Similarly, when the die diameter increased from 8.0mm to 10.0mm, the interlock also showed a smaller decreasing speed with a small depth die (e.g.  $H_1=1.6$ mm) than with a larger one (e.g.  $H_1=2.0$ mm). However, considering the relatively small changing range (from 0.51mm to 0.555mm)

of the  $T_{\min}$  in **Fig. 19** (b) and the prediction accuracy of the regression model (MAE=0.029mm), the interaction effects on the  $T_{\min}$  were not confident to be evaluated and therefore not discussed in detail.

The simulated joint cross-sectional profiles at the points a~i in **Fig. 19** are presented in **Fig. 20**. A good agreement between the predicted results from the developed regression models and the FEA simulation model was also found. For a given die diameter, the increase of the die depth was accompanied by the decreased interlock and the almost unchanged  $T_{\min}$ . For a given die depth, the increased die diameter also lead to the decreased interlock and the almost constant  $T_{\min}$ . It is worth mentioning that both of the interlock and the  $T_{\min}$  varied within narrow ranges (i.e. 0.18mm and 0.045mm respectively) in **Fig. 19** than that in **Fig. 13** or **Fig. 17**. This indicates the smaller influences of the die diameter and depth on the SPR joint quality than that of the rivet length under the studied joint configurations.

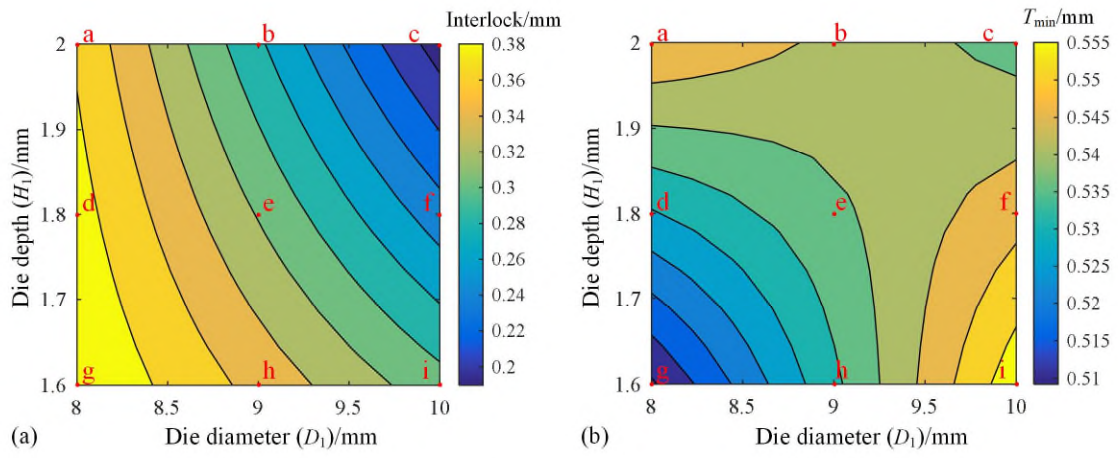


**Fig. 19** Contour graphs of (a) the interlock and (b) the  $T_{\min}$  with different die diameters and depths (Rivet length=5.0mm)

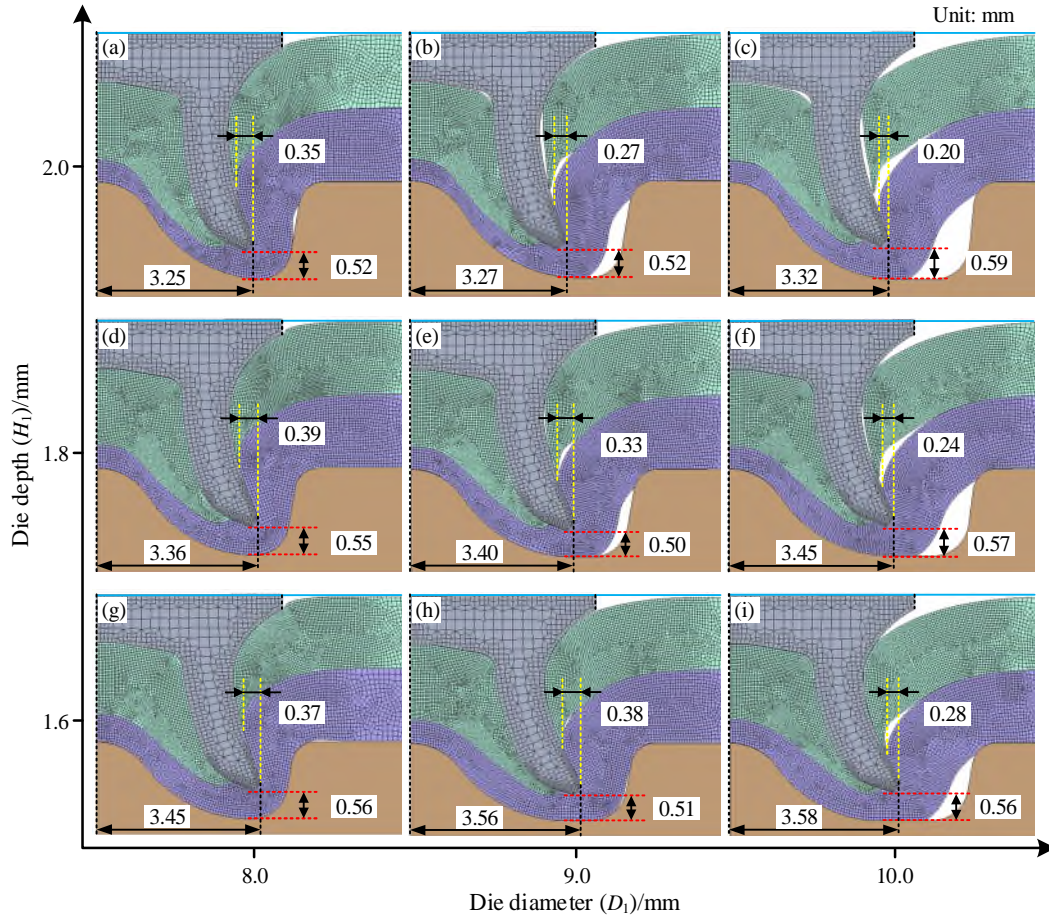


**Fig. 20** Simulated joint cross-sectional profiles with different die diameters and depths (Rivet length=5.0mm)

The relationship between the formation of the interlock and the Die-to-Rivet volume ( $R$ ) was discussed previously, hence here will not discuss further. It is worth mentioning that the maximum interlock was achieved on the lower left corner of the **Fig. 19** (a) with the  $R$  closer to 1.0, while the minimum interlock was observed on the upper right corner of the **Fig. 19** (a) when the  $R$  equals to 1.59. In addition, such interaction effect also revealed that when the  $R$  value is less than 1.0, the increment of the  $R$  value could lead to a larger interlock, but when the  $R$  value is greater than 1.0, the increment of the  $R$  value could result in a smaller interlock. Except for the  $R$ , the die depth is also very important because it directly determines when the rivet shank started flaring rapidly. Therefore, the die depth should be considered together with the  $R$  during the selection of rivet and die. For the studied material combination, the shallower die is better for the formation of the interlock. For other material combinations, further study is required.

## 5 Conclusions

In this study, simple but effective multiple regression models were proposed to predict the SPR joint quality. The interaction effects between the rivet and die parameters on the joint quality were graphically analysed and digitally validated. The main conclusions were listed as below:



1. The developed multiple regression models **were proved** effective to describe the relationships between the joining parameters and the SPR joint quality. **The MAE values** between the experimental results and regression predictions for the interlock and the  $T_{\min}$  **were 0.047mm and 0.053mm respectively, and the corresponding MAPE were 10.4% and 12.3% under the studied joint configurations.**
2. It is straightforward to analyse the interaction effects between the joining parameters on the joint quality by observing the contour graphs drawn from the developed regression models. Significant interaction effects between the rivet length, the die diameter and the die depth were identified on the interlock, but not on the  $T_{\min}$  within the studied range.
3. By affecting the deformation behaviours of the rivets and sheets, the Die-to-Rivet volume ratio ( $R$ ) significantly influenced the magnitude and changing trend of the interlock when with varying joining parameters. A larger interlock was more likely to be achieved when the  $R$  was close to 1.0.

The introduction of the regression model is the first step towards more complicated and more industrial applications by involving more joining parameters, such as the sheet thickness, the rivet hardness, etc. In addition, it also offers the possibility to optimize the SPR joint quality by using the mathematic model together with other optimization algorithms.

**Acknowledgement** The authors would like to thank Dr. Matthias Wissling, Paul Bartig and their team members from Tucker GmbH for their supports during the laboratory tests.

**Funding** This research is funded by Jaguar Land Rover Limited.

**Authors' contributions** Huan Zhao, Li Han, Yunpeng Liu and Xianping Liu worked together to conceive this research. Huan Zhao designed the experiments, analysed the data and completed the original draft. Li Han supervised the experiments and provided critical paper revisions. Yunpeng Liu supported with the FEA simulation model and manuscript revision. Xianping Liu is the project leader and participated in the paper revision. All authors read and approved the final manuscript.

**Availability of data and materials** Not applicable

## Compliance with Ethical Standards

**Competing Interests** The authors declare that they have no conflict of interest.

**Ethical Approval** Not applicable

**Consent to Participate** Not applicable

**Consent to Publish** Not applicable



## References

1. Reinhert P (2004) The new Jaguar XJ - The first all aluminium car in monocoque design. *Alum Int Today* 16:21–24
2. Abe Y, Kato T, Mori K (2006) Joinability of aluminium alloy and mild steel sheets by self piercing rivet. *J Mater Process Technol* 177:417–421. <https://doi.org/10.1016/j.jmatprotec.2006.04.029>
3. He X, Zhao L, Deng C, et al (2015) Self-piercing riveting of similar and dissimilar metal sheets of aluminum alloy and copper alloy. *Mater Des* 65:923–933. <https://doi.org/10.1016/J.MATDES.2014.10.002>
4. Kotadia HR, Rahn timer A, Sohn IR, et al (2019) Performance of dissimilar metal Self-Piercing Riveting (SPR) joint and coating behaviour under corrosive environment. *J Manuf Process* 39:259–270. <https://doi.org/10.1016/J.JMAPRO.2019.02.024>
5. Han L, Thornton M, Shergold M (2010) A comparison of the mechanical behaviour of self-piercing riveted and resistance spot welded aluminium sheets for the automotive industry. *Mater Des* 31:1457–1467. <https://doi.org/10.1016/J.MATDES.2009.08.031>
6. Li D, Chrysanthou A, Patel I, Williams G (2017) Self-piercing riveting-a review. *Int J Adv Manuf Technol* 92:1777–1824. <https://doi.org/10.1007/s00170-017-0156-x>
7. He X, Gu F, Ball A (2012) Recent development in finite element analysis of self-piercing riveted joints. *Int J Adv Manuf Technol* 58:643–649. <https://doi.org/10.1007/s00170-011-3414-3>
8. Haque R (2018) Quality of self-piercing riveting (SPR) joints from cross-sectional perspective: A review. *Arch Civ Mech Eng* 18:83–93. <https://doi.org/10.1016/j.acme.2017.06.003>
9. Kam DH, Jeong TE, Kim MG, Shin J (2019) Self-piercing riveted joint of vibration-damping steel and aluminum alloy. *Appl Sci* 9:. <https://doi.org/10.3390/app9214575>
10. Zhang X, He X, Xing B, et al (2020) Quasi-static and fatigue characteristics of self-piercing riveted joints in dissimilar aluminium-lithium alloy and titanium sheets. *J Mater Res Technol.* <https://doi.org/10.1016/j.jmrt.2020.03.095>
11. Han L, Thornton M, Li D, Shergold M (2010) Effect of setting velocity on self-piercing riveting process and joint behaviour for automotive applications. *SAE Tech Pap.* <https://doi.org/10.4271/2010-01-0966>
12. Haque R, Beynon JH, Durandet Y (2012) Characterisation of force-displacement curve in self-pierce riveting. *Sci Technol Weld Join* 1718:. <https://doi.org/10.1179/1362171812Y.00000000036>
13. Sun X, Khaleel MA (2005) Performance Optimization of Self-Piercing Rivets Through Analytical Rivet Strength Estimation. *J Manuf Process* 7:83–93. [https://doi.org/10.1016/S1526-6125\(05\)70085-2](https://doi.org/10.1016/S1526-6125(05)70085-2)

14. Xu Y (2006) Effects of factors on physical attributes of self-piercing riveted joints. *Sci Technol Weld Join* 11:666–671. <https://doi.org/10.1179/174329306X131866>
15. Ma Y, Lou M, Li Y, Lin Z (2018) Effect of rivet and die on self-piercing rivetability of AA6061-T6 and mild steel CR4 of different gauges. *J Mater Process Technol* 251:282–294. <https://doi.org/10.1016/J.JMATPROTEC.2017.08.020>
16. Li DZ, Han L, Shergold M, et al (2013) Influence of Rivet Tip Geometry on the Joint Quality and Mechanical Strengths of Self-Piercing Riveted Aluminium Joints. *Mater Sci Forum* 765:746–750. <https://doi.org/10.4028/www.scientific.net/MSF.765.746>
17. Mucha J (2011) A study of quality parameters and behaviour of self-piercing riveted aluminium sheets with different joining conditions. *Stroj Vestnik/Journal Mech Eng* 57:323–333. <https://doi.org/10.5545/sv-jme.2009.043>
18. Han SL, Li ZY, Gao Y, Zeng QL (2014) Numerical study on die design parameters of self-pierce riveting process based on orthogonal test. *J Shanghai Jiaotong Univ* 19:308–312. <https://doi.org/10.1007/s12204-014-1504-8>
19. Jäckel M, Falk T, Landgrebe D (2016) Concept for Further Development of Self-pierce Riveting by Using Cyber Physical Systems. *Procedia CIRP* 44:293–297. <https://doi.org/10.1016/j.procir.2016.02.073>
20. Bhushan RK (2013) Optimization of cutting parameters for minimizing power consumption and maximizing tool life during machining of Al alloy SiC particle composites. *J Clean Prod* 39:242–254. <https://doi.org/10.1016/j.jclepro.2012.08.008>
21. Singh B, Ahuja N (2002) Development of controlled-release buccoadhesive hydrophilic matrices of Diltiazem hydrochloride: Optimization of bioadhesion, dissolution, and diffusion parameters. *Drug Dev Ind Pharm* 28:431–442. <https://doi.org/10.1081/DDC-120003004>
22. Anawa EM, Olabi AG (2008) Using Taguchi method to optimize welding pool of dissimilar laser-welded components. *Opt Laser Technol* 40:379–388. <https://doi.org/10.1016/j.optlastec.2007.07.001>
23. Bitondo C, Prisco U, Squilace A, et al (2011) Friction-stir welding of AA 2198 butt joints: Mechanical characterization of the process and of the welds through DOE analysis. *Int J Adv Manuf Technol* 53:505–516. <https://doi.org/10.1007/s00170-010-2879-9>
24. Zhao D, Wang Y, Liang D, Zhang P (2016) Modeling and process analysis of resistance spot welded DP600 joints based on regression analysis. *Mater Des.* <https://doi.org/10.1016/j.matdes.2016.08.038>
25. Carandente M, Dashwood RJ, Masters IG, Han L (2016) Improvements in numerical simulation of the SPR process using a thermo-mechanical finite element analysis. *J Mater Process Technol* 236:148–161. <https://doi.org/10.1016/J.JMATPROTEC.2016.05.001>

26. He X, Xing B, Zeng K, et al (2013) Numerical and experimental investigations of self-piercing riveting. *Int J Adv Manuf Technol* 69:715–721. <https://doi.org/10.1007/s00170-013-5072-0>
27. Liu Y, Li H, Zhao H, Liu X (2019) Effects of the die parameters on the self-piercing riveting process. *Int J Adv Manuf Technol* 105:1–16. <https://doi.org/10.1007/s00170-019-04567-4>